FEM Simulations to Study the Effects of Laser Power and Scan Speed on Molten Pool Size in Additive Manufacturing

Yee-Ting Lee, Jyun-Rong Zhuang, Wen-Hsin Hsieh, An-Shik Yang

Abstract—Additive manufacturing (AM) is increasingly crucial in biomedical and aerospace industries. As a recently developed AM technique, selective laser melting (SLM) has become a commercial method for various manufacturing processes. However, the molten pool configuration during SLM of metal powders is a decisive issue for the product quality. It is very important to investigate the heat transfer characteristics during the laser heating process. In this work, the finite element method (FEM) software ANSYS® (work bench module 16.0) was used to predict the unsteady temperature distribution for resolving molten pool dimensions with consideration of temperature-dependent thermal physical properties of TiAl6V4 at different laser powers and scanning speeds. The simulated results of the temperature distributions illustrated that the ratio of laser power to scanning speed can greatly influence the size of molten pool of titanium alloy powder for SLM development.

Keywords—Additive manufacturing, finite element method, molten pool dimensions, selective laser melting.

I. INTRODUCTION

SLM is one of elementary AM techniques, employing a moving laser heat source to completely melt a powder layer for producing higher-density units. SLM is not only able to directly fabricate dense metal parts in a very short time, but also this method has been extensively implemented to rapid prototyping and precise manufacturing field [1]. The process parameters in SLM are the key issues to the final mechanical properties of produced parts [2]. Previous studies have provided a theoretical and technical basis via exploring the links between SLM process parameters and geometrical characteristics of the molten pool dimensions [3]-[6]. Lately, various numerical models have been established to predict the effects of processing parameters consisting of the moving heat energy source intensity, scanning speed, thickness of the powder layer on the heat-affected zone, melt pool extent and stress distribution during SLM [7]-[9]. In this work, the FEM software ANSYS® (workbench module 16.0) was utilized to forecast the unsteady temperature field for analyzing the effects of laser powers and scanning speeds on the configuration of the molten pool with the consideration of latent heat of phase change and temperature-dependent thermal physical properties of TiAl6V4 powder bed. The simulated results of the temperature distributions revealed that the ratio of laser power to scanning speed can greatly influence the molten pool dimensions of titanium alloy powder for SLM process.
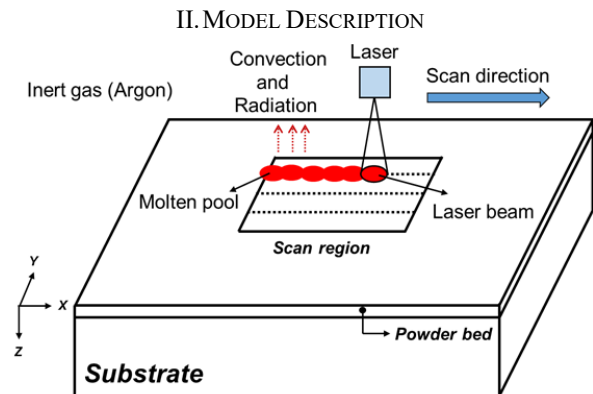
II. MODEL DESCRIPTION

Fig. 1 Schematic of the heat transfer mechanism for laser heating of metal powders

Fig. 1 presents a schematic diagram describing the thermal behavior of SLM process. The powder was selectively melted under an inert atmosphere (i.e. Argon (Ar) in this case) by a laser beam. The laser irradiation heat will be dissipated to the surroundings by conduction, convection and radiation to the solid metal, metal powder, and shielding gas. The remainder of laser energy is absorbed by the powder layer and results in localized melting with the formation of a molten pool. The metallurgical bonding is produced between the adjacent tracks and the adjacent layers by rapid solidification after the moving laser heat source leaves. This research used ANSYS® software (Workbench v16.0) to conduct the thermo-mechanical coupling analysis for exploring the thermal essentials of laser melting development. A 3D FEM model, covering all detailed structure parts, was constructed using ANSYS® for the predictions of the time-varying temperature field during the SLM process. Fig. 2 shows the schematic depicting an established 3D FEM model and laser scan strategy during SLM process. The laser scan area on a Ti6Al4V powder layer had a length of 3.0 mm, a width of 3.0 mm, and a depth of 0.03 mm. The dimensions of powder bed were 3.0 mm in length, 3.0 mm in width, and 1.0 mm in depth, respectively. In practice, the layer was processed progressively in the pattern of three scanning tracks, as

Yee-Ting Lee and An-Shik Yang are with Department of Energy and Refrigerating Air-Conditioning Engineering, National Taipei University of Technology, Taipei 10608, Taiwan (phone: 886-2-2771-2171 ext. 3523; fax: 886-2- 2731-49191; e-mail: asyang@ntut.edu.tw).

Jyun-Rong Zhuang is with Graduate School of Information, Production and Systems, Waseda University in Fukuoka, Japan.

Wen-Hsin Hsieh is with the Department of Mechanical Engineering, National Chung-Cheng University, Chiayi 621, Taiwan (phone: 886-5-242-8170; fax: 886-5-272-0589; e-mail: imewhh@ccu.edu.tw).

World Academy of Science, Engineering and Technology
International Journal of Mechanical and Mechatronics Engineering
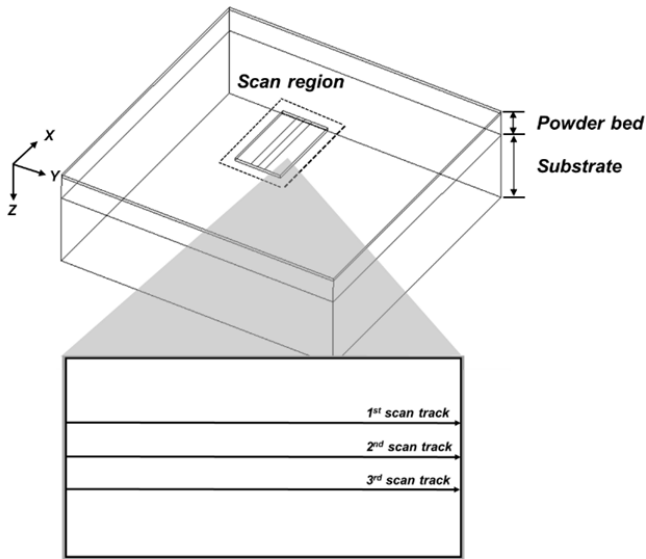Vol:11, No:7, 2017

depicted in Fig. 2.

Fig. 2 Schematic depicting an established 3D FEM model and laser scan strategy during SLM process

The laser heat source acting on the top surface of Ti6Al4V powder bed was modeled as a mobile heat flux following a Gaussian distribution along the axial axis with a constant speed. Alternatively, the target materials were assessed by monitoring the temperature field during simulations. The laser processing parameters in SLM are listed in Table I.

TABLE I
LASER PROCESSING PARAMETERS OF SLM PROCESS

Symbol	Parameter	Value
P	Laser power	95 W
V	Scan speed,	210 mm/s
Ω	Laser spot radius	0.05 mm
l	Track length	0.85 mm
d	Hatch spacing	0.075 mm
Nt	Track number	3
δ	Powder layer thickness	0.03 mm
A	Laser absorptivity of powder	0.3
h	Total heat transfer coefficient	80 W/ m^2 -K

III. COMPUTATIONAL ANALYSIS

This study used ANSYS® simulation software (Release 16.0) to build a 3D thermal-structure model for probing the thermal behavior and predicting the time dependent temperature field associated with SLM progression. The laser beam produced the localized heating of the powder bed, causing the transfer of heat energy to metal material governed by conductive heat transfer. Essentially, the transient 3D heat conduction equation can be described as below [10].

$$\rho c \frac{\partial T}{\partial t} - \nabla^T (k \cdot \nabla T) + \dot{Q} = 0 \qquad (1)$$

The symbols ρ, c, T, t, k, Q, and ∇ denote the material density, specific heat capacity, temperature of the powder system, interaction time between the laser beam and powder, thermal conductivity, heat generated per volume within the component, and the spatial gradient operator, respectively. The following expression is used to specify the thermal boundary conditions for powder, liquid, and solid [11].

$$k \frac{\partial T}{\partial n} - q + q_c + q_r = 0, \ (x,y,z) \in S, \qquad (2)$$

where S represents the surfaces attached to imposed heat fluxes (convection and radiation), n is the normal vector of S, q is the input heat flux from the laser energy source with a description of q given later, q_c and q_r are the heat loss because of natural convection and radiation of the fluid around the powder bed. The induced melting of material was usually achieved using a moving Gaussian distributed source term as a thermal energy source during the SLM process. The distribution of laser beam intensity follows nearly a Gaussian relation, as mathematically presented in the following [12].

$$q = \frac{2 AP}{\pi R^2} \exp \left(- \frac{2 r^2}{R^2} \right) \qquad (3)$$

where A is the laser energy absorptivity of Ti6Al4V powder as listed in Table I, P is the laser power, R designates the radius of the Gaussian heat source, showing the distance from the center of laser beam to the point at which the energy reduced to its $1/e^2$, and r is the radial distance from a point on the powder bed surface to the center of the laser spot. The latent heat of fusion should be considered in computations. The enthalpy change caused by an increase in specific heat is utilized to calculate the latent heat of fusion at the melting point as below [13].

$$\Delta H = \rho T_m (\Delta c). \qquad (4)$$

where the term ΔH is the enthalpy change, Δc is the specific heat capacity change and T_m is the melting point. The effective thermal conductivity of loose metallic powders is dominated by gas in the pores influencing the accuracy of SLM simulation results. Rombouts et al. [14] reported that the effective thermal conductivity of a powder bed is independent of material but depends on the size and morphology of particles, void fraction, and thermal conductivity of the gas. Thus, the effective thermal conductivity of the powder bed, k_{eff}, is determined as follows [15].

$$\frac{k_{eff}}{k_f} = \left(1 - \sqrt{1-\phi}\right) \left(1 + \frac{\phi k_r}{k_f}\right) + \sqrt{1-\phi} \left[\frac{2}{1 - \frac{k_f}{k_s}} \left(\frac{1}{1 - \frac{k_f}{k_s}} \ln\left(\frac{k_s}{k_f}\right) - 1 \right) + \frac{k_r}{k_f} \right] \cdot$$

$$(5)$$

where the symbol ϕ is the porosity of the powder bed. The signs k_f, k_s and k_r correspond to the thermal conductivity of the fluid (i.e. argon in this case). The thermal physical properties of

World Academy of Science, Engineering and Technology
International Journal of Mechanical and Mechatronics Engineering
Vol:11, No:7, 2017

TiAl6V4 are illustrated in Table II [16], where the sudden changes of thermal physical properties can be clearly observed due to the transition from α phase to β phase at 950 °C and the melting point of 1933 °C. Fig. 3 exhibits the numerical grids for reproducing the laser heating of a powder bed in SLM simulations with the total grids of 65728 points. The mesh setup consisted of two sections: the powder layer and dense substrate. In practice, finer grids have been arranged in the areas near the scanning region of powder layer to describe the rapid variations of temperature field. This study generated ANSYS® Solid 70 hexahedral elements for the powder bed, whereas tetrahedral elements were used in the substrate with a time step of 2×10^{-5} s. Hence, the 3D FEM model was meshed into 43881 elements (with the nodes of 51986) for the powder layer and 21847 elements (with the nodes of 31592) for the substrate layer, respectively. It generally required around 70 minutes of central processing unit (CPU) time on an Intel® Xeon® E5-2670v3-2.3 GHz×2 (192 GB RAM) workstation to attain a solution.
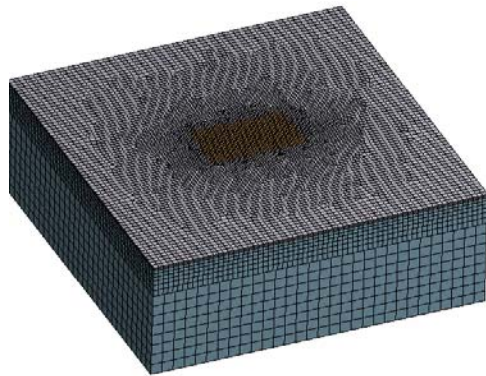

Fig. 3 Numerical grids for reproducing laser heating of a powder bed in SLM simulations

IV. Results and Discussion

Considering typical temperature distributions of melt pool along the laser scanning path (the laser beam is moving from left to right for this case), Fig. 4 illustrates the time sequences of predicted temperature contours on the top surface of 3D melt pool at various locations including (a) the start of the first track (Point 1), (b) the center of the second track (Point 2) and (c) the end of the third track (Point 3) for the laser power of 95 W and scanning speed of 210 mm/s during SLM of TiAl6V4 powder: top view and side view. The dotted line on the graphs indicated the isotherm curve corresponding to the melting temperature of Ti6Al4V (i.e. 1933 K) on the top surface. It can be observed that the maximum temperature on the top surface within this specific contour indicated a liquid state due to its temperature above the melting point, producing an asymmetry melt pool characterized by a series of ellipses. The laser heat was mainly transferred downwards and backwards to generate the intensive isothermal contours of front ellipses as compared to those at the back side because of higher thermal conductivity and thermal accumulation.

TABLE II
VARIATION OF THERMO-PHYSICAL PROPERTIES FOR TiAl6V4 WITH
TEMPERATURE [16]

Temp. [°C]	Density [kg/m³]	Specific Heat [J/kg-K]	Thermal Conductivity [W/m-K]
25	4420	546	7
100	4406	562	7.45
200	4395	584	8.75
300	4381	606	10.15
400	4366	629	11.35
500	4350	651	12.6
600	4336	673	14.2
700	4324	694	15.5
800	4309	714	17.8
900	4294	734	20.2
994	4282	753	22.7
996	4282	693	19.3
1100	4267	660	21
1200	4252	678	22.9
1300	4240	696	23.7
1400	4225	714	24.6
1500	4205	732	25.8
1600	4198	750	27
1649	4189	759	28.4
1651	3920	1007	83.5
1700	3886	831	83.5
1800	3818	831	83.5
1900	3750	831	83.5

At Point 1 in Fig. 4 (a) with the laser spot located at the start of the first track, the predicted peak temperature of powder layer was 3752.8 K due to low conductivity of material in the region under laser irradiation, exceeding the Ti6Al4V melting point of 1933 K to cause the occurrence of localized melting of powder. Nonetheless, this peak temperature dropped with increasing move distance of laser spot because of the heat conduction into the dense substrate with a high conductivity. The melt pool size was around 98.61 μm long, 95.83 μm wide and 11.66 μm deep, respectively. At Point 2 in Fig. 4 (b) with the laser beam reached the center of the second scan track, the highest temperature of the melt pool decreased to 2479.3 K. In addition, the melt pool dimensions were 158.5 μm×130.53 μm× 46.61 μm. As the laser spot further moved to the end of the third track (Point 3, Fig. 4 (c)), the temperature contours were noted to be more intense at the front side than those at the back side of the ellipses with an increase in the maximum temperature of the powder bed to 2488.5 K. The melt pool dimensions of 169.44 μm×137.15 μm×52.5 μm were relatively larger than those at the cases of Point 1 and Point 2. It could be attributed that the heat accumulation had an effect on the temperature field of the next track. The combined results of greater heat accumulation and a longer interaction time of the laser beam with the powder bed also produced a higher temperature at the end for the last track. Fig. 5 illustrates the predictions of length, width and depth of melt pool in SLM of TiAl6V4 powder with different processing parameters: (a) laser power of 75-150 W (at scanning speed of 210 mm/s,); (b) scanning speed of 100-400 mm/s (at laser power of 95 W). In calculations, the preheating temperature and hatch space of TiAl6V4 powder bed were 110

World Academy of Science, Engineering and Technology
International Journal of Mechanical and Mechatronics Engineering
Vol:11, No:7, 2017

°C and 0.075 mm for the baseline state. Overall, the length, width and depth of the melt pool increased with the laser power on the powder layer due to more energy transferred into the heat affected zone. The laser power raised from 75 to 150 W at a scanning speed of 210 mm/s led to obvious expanding of the melt pool size. Increasing laser power can produce a high operating temperature of the powder layer in SLM, and enhance liquid formation of melt pool to enlarge the melt pool extent. It was also observed in Fig. 5 (a) that the associated length, width and depth increased from 147.5 µm×116.2 µm×36.4 µm to 243.5 µm×183.4 µm×86.0 µm, respectively. In contrast, the simulated results in Fig. 5 (b) evidently indicated the decline of three dimensions of the melt pool with the increment of the applied scan speed. When the scanning speed was increased from 100 to 400 mm/s at a fixed laser power of 95 W, the length of the melt pool decreased from 208.2 to 157.0 µm. Besides, the associated width/depth reduced from 168.1/73.3 µm to 115.6/35.4 µm. Under higher scan speed conditions, there was no sufficient time for the event of melting process to produce a long thin melt pool over the track, causing that most materials within this region still remained in a state of non-melted powder.
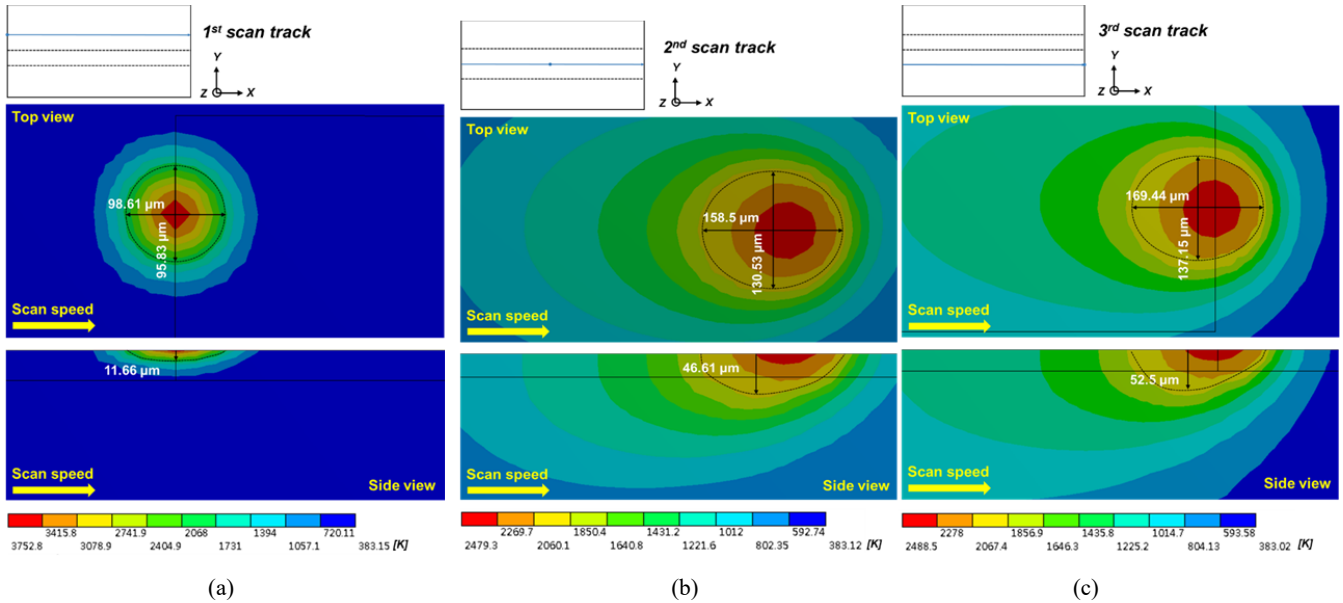

Fig. 4 Time sequences of predicted temperature contours on the top surface of 3D melt pool at various locations including (a) the start of the first track (Point 1), (b) the center of the second track (Point 2) and (c) the end of the third track (Point 3) for the laser power of 95 W and scanning speed of 210 mm/s during SLM of TiAl6V4 powder: top view and side view
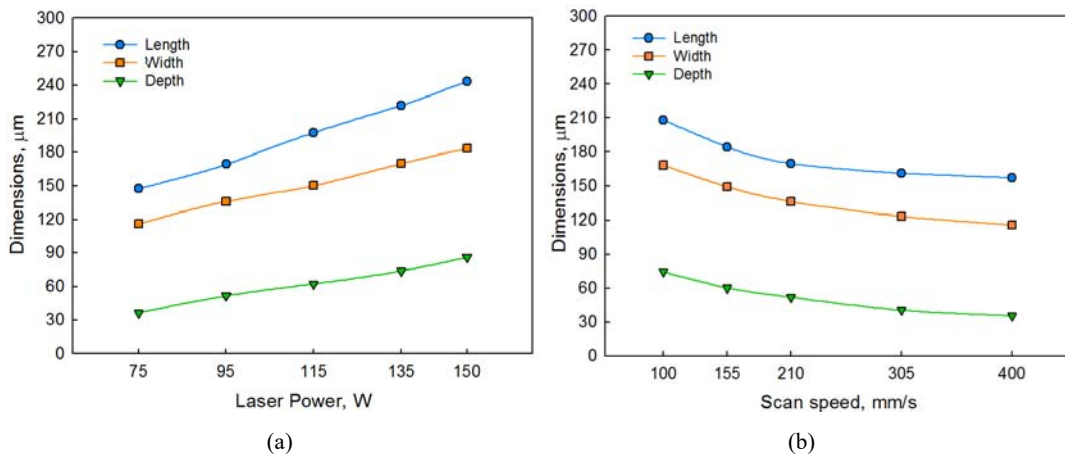

Fig. 5 Predictions of length, width and depth of the melt pool in SLM of TiAl6V4 powder with different processing parameters: (a) laser power of 75-150 W (at scanning speed of 210 mm/s,); (b) scanning speed of 100-400 mm/s (at laser power of 95 W)

V. CONCLUSION

Taking the mobile Gaussian distribution of the heat flux and the temperature-dependent thermophysical parameters into consideration, a 3D FEM model was established to investigate thermal behaviors during SLM of Ti6Al4V powder. The laser beam moving from the start to the end of tracks leads to an increase in length, width, and depth of the molten pool. This is mainly owing to the heat accumulation effect and higher energy

World Academy of Science, Engineering and Technology
International Journal of Mechanical and Mechatronics Engineering
Vol:11, No:7, 2017

losses through the conduction than the convection and radiation during SLM. The dimensions of length, width and depth of melt pool increased from 147.5, 116.2 and 36.5 µm to 243.5, 183.4 and 86.0 µm, respectively, as the laser power raised from 75 W to 150 W. Alternatively, the scanning speed elevated from 100 to 400 mm/s, the length, width and depth of melt pool reduced from 208.2 µm×168.1 µm×73.3 µm to 157.0 µm× 115.6 µm× 35.4 µm, respectively. Consequently, it can be not easy to obtain sufficient metallurgical bonding between neighboring regions because of relatively smaller dimensions of the molten pool at a relatively higher scanning speed (i.e. 400 mm/s) or a lower laser power (75 W).

REFERENCES

[1] I. Yadroitsev, I. Yadroitsava, P. Bertrand, and I. Smurov, "Factor analysis of selective laser melting process parameters and geometrical characteristics of synthesized single tracks", Rapid Prototyp. J., vol. 18, pp. 201–208, 2012.

[2] A. Hussein, L. Hao, C. Yan, and R. Everson, "Finite element simulation of the temperature and stress fields in single layers built without-support in selective laser melting", Mater. Des., vol. 52, pp. 638–647, 2013.

[3] I. Yadroitsev, P. Krakhmalev, and I. Yadroitsava, "Selective laser melting of Ti6Al4V alloy for biomedical applications: Temperature monitoring and microstructural evolution", J. Alloy. Compd., vol. 583, pp. 404–409, 2014.

[4] D. D. Gu, Y. C. Hagedorn, W. Meiners, G. Meng, R. J. S. Batista, K. Wissenbach, and R. Poprawe, "Densification behavior, microstructure evolution, and wear performance of selective laser melting processed commercially pure titanium", Acta Mater., vol. 60, pp. 3849–3860, 2012.

[5] K. Dai, and L. Shaw, "Finite element analysis of the effect of volume shrinkage during laser densification", Acta Mater., vol. 53, pp. 4743–4754, 2005.

[6] D. D. Gu, and Y. Shen, "Balling phenomena in direct laser sintering of stainless steel powder: metallurgical mechanisms and control methods", Mater. Des., vol. 30, pp. 2903–2910, 2009.

[7] Y. W. Zhang, A. Faghri, C. W. Buckley, and T. L. Bergman, "Three-dimensional sintering of two-component metal powders with stationary and moving laser beams", J Heat Transfer, vol. 122, pp. 150–158, 2000.

[8] I. A. Roberts, C. J. Wang, R. Esterlein, M. Stanford, and D.J. Mynors, "A three-dimensional finite element analysis of the temperature field during laser melting of metal powders in additive layer manufacturing", Int. J. Mach. Tools Manuf., vol. 49, pp. 916–923, 2009.

[9] A. V. Gusarov, and I. Smurov, "Modeling the interaction of laser radiation with powder bed at selective laser melting", Phys Procedia, vol. 5, pp. 381–394, 2010.

[10] H. S. Carslaw, and J.C. Jaeger, "Conduction of Heat in Solids", 2nd ed, Oxford University Press, Oxford, 1986.

[11] G. Germain, F. Morel, and J. L. Lebrun, "A Morel, Machinability and surface integrity for a bearing steel and a titanium alloy in laser assisted machining", Laser Eng., vol. 17, pp. 329–344, 2007.

[12] J. Yin, H.H. Zhu, L. D. Ke, W. J. Lei, C. Dai, and D. L. Zuo, "Simulation of temperature distribution in single metallic powder layer for laser micro-sintering", Comput. Mater. Sci., vol. 53, pp. 333–339, 2012.

[13] Y. Huang, L. J. Yang, X. Z. Du, and Y. P. Yang, "Finite element analysis of thermal behavior of metal powder during selective laser melting", Int. J. Therm. Sci., vol. 104, pp. 146-157, 2016.

[14] M. Rombouts, L. Froyen, A. V. Gusarov, E. H. Bentefour, and C. Glorieux, "Light extinction in metallic powder beds: correlation with powder structure", J Appl. Phys., vol. 98, 2005.

[15] S.S. Sih, and J.W. Barlow, "The prediction of the emissivity and thermal conductivity of powder beds", Part. sci. technol., vol. 22, pp. 427–440, 2004.

[16] V. Fallah, M. Alimardani, S. Corbin, and A. Khajepour, "Temporal development of melt-pool morphology and clad geometry in laser powder deposition", Comput. Mater. Sci., vol. 50, pp. 2124–2134, 2011.

Yee-Ting Lee received her Master of Science degree in the Department of Energy and Refrigerating Air-Conditioning Engineering at National Taipei University of Technology, Taiwan. Her primary research interests include the fluid dynamics, heat transfer, selecting laser melting process analysis and CFD simulations.

Jyun-Rong Zhuang is currently pursuing Ph. D. degree at the Graduate School of Information, Production and Systems, Waseda University in Fukuoka, Japan. His research interests include the design improvement to minimize thermal errors of high speed machine tools, selecting laser melting process analysis and ANSYS simulation analysis.

Wen-Hsin Hsieh received his M.S. and Ph. D. in mechanical engineering from the Pennsylvania State University, University Park, PA, USA in 1987. He is currently Dean of the College of Engineering and professor of the Department of Mechanical Engineering at National Chung Cheng University, Taiwan. His research interests are in the fields of bio-chip, microfluidics, combustion and heat transfer.

An-Shik Yang received his Bachelor of Science (1982) and Master of Science (1984) degrees from the National Tsing Hua University in Taiwan, and Ph.D. (1993) degree from the Pennsylvania State University in USA. He is currently a professor with the Department of Energy and Refrigerating Air-Conditioning Engineering at National Taipei University of Technology (NTUT) in Taipei, Taiwan. Dr. Yang is an Associate Fellow of American Institute of Aeronautics and Astronautics (AIAA). His research interests include the microfluidic design, environmental fluid mechanics, and heat transfer.